Atmospheric Research 248 (2021) 105190

Contents lists available at ScienceDirect

Atmospheric Research

journal homepage: www.elsevier.com/locate/atmosres

Spatial and temporal variations of atmospheric chemical condition in the Southeastern U.S.

Bin Cheng[a], Lingjuan Wang-Li[a,*], John Classen[a], Nicholas Meskhidze[b], Peter Bloomfield[c]

[a] Department of Biological and Agricultural Engineering, North Carolina State University, Raleigh, NC 27695, USA
[b] Department of Marine Earth and Atmospheric Science, North Carolina State University, Raleigh, NC 27685, USA
[c] Department of Statistics, North Carolina State University, Raleigh, NC 27695, USA

ARTICLE INFO

Keywords:
AFOs NH_3 emissions
Chemical condition
Precursor gases
Secondary inorganic $PM_{2.5}$

ABSTRACT

Animal feeding operations (AFOs) are the largest ammonia (NH_3) emission sources in the United States (U.S.). However, the impact of NH_3 emissions from AFOs on the formation of secondary inorganic $PM_{2.5}$ ($iPM_{2.5}$) has not been well understood and systematically assessed. Under the Southeastern Aerosol Research and Characterization (SEARCH) Network, the hourly concentrations of $iPM_{2.5}$ chemical compositions and its precursor gases as well as meteorological data were measured at eight urban/nonurban sites labeled as JST/YRK, BHM/CTR, GFP/OAK, and PNS/OLF during 1998–2016. Using the SEARCH data, this research investigated the spatiotemporal variations of atmospheric chemical conditions in those rural and urban areas. The spatiotemporal variations of atmospheric chemical conditions at the eight sites are characterized by four parameters, including (1) gas ratio (GR), (2) gas-phase NH_3 molar fraction (NH_3/NH_x), (3) total available NH_3 (gaseous ammonia + aerosol ammonium) to sulfate (SO_4^{2-}) molar ratio (TA/TS), and (4) $PM_{2.5}$ ammonium + nitrate to total $PM_{2.5}$ mass ratio ($AN/PM_{2.5}$). Results indicate that the NH_3 emissions from AFOs may explain the greater values of GR, NH_3/NH_x, and TA/TS in the wind directions coming from AFOs at YRK and OAK rural sites than the other wind directions. In the wind directions coming from AFOs at YRK and OAK, NH_3 was in excess of fully neutralizing acidic gases, more NH_3 stayed in gas phase than those in other wind directions, and both ammonium sulfate and ammonium nitrate existed in $iPM_{2.5}$. The upward trend in NH_3/NH_x indicates that gas-particle partitioning ofNH_3–NH_4^+ shifted toward gas phase, while the downward trend in $AN/PM_{2.5}$ may implicate that smaller fraction of $PM_{2.5}$ was directly NH_3 sensitive. Understanding of the spatiotemporal variations of atmospheric chemical condition provides insights to improve our understanding of $iPM_{2.5}$ formation under rural and urban conditions, the reduction in sulfur dioxide (SO_2) and nitrogen oxides (NO_x) emissions resulted in the reduction of $iPM_{2.5}$ formation despite the increase in NH_3 emissions in the Southeastern U.S.

1. Introduction

Particulate matter with aerodynamic equivalent diameter less than or equal to 2.5 μm (i.e., $PM_{2.5}$) has gained intensive attention due to its adverse health and visibility degradation effects (Cambra-Lopez et al., 2010; Li et al., 2018; Ma et al., 2011; Pope III et al., 2009; Pui et al., 2014; Zhang et al., 2015). $PM_{2.5}$ may be formed through different processes. Primary $PM_{2.5}$ is directly emitted from sources, while secondary $PM_{2.5}$ is formed through chemical reactions of various precursor gases in homogeneous and/or heterogeneous processes (Hinds, 1998; Seinfeld and Pandis, 2006; Wang et al., 2006; USEPA, 2020). In ambient air, ammonia (NH_3) as the major alkaline gas, may react with acidic gases, i.e., nitric acid (HNO_3) and sulfuric acid (H_2SO_4), to form ammonium (NH_4^+) salts, a.k.a. secondary inorganic $PM_{2.5}$ ($iPM_{2.5}$), in a process called thermodynamic equilibrium gas-particle partitioning ofNH_3–NH_4^+ (Huy et al., 2019; Seinfeld and Pandis, 2006; Wang-Li, 2015; Zhang et al., 2008). Secondary $iPM_{2.5}$ constitutes a significant fraction of atmospheric $PM_{2.5}$ in the United States (U.S.) (Bell et al., 2007; Cheng et al., 2019; Cheng and Wang-Li, 2019a, 2019b; Walker et al., 2004), in China (Geng et al., 2017; Liu et al., 2018; Meng et al., 2018; Tian et al., 2016; Xu et al., 2016), in India (Sharma et al., 2007), in Italy (Perrone et al., 2019; Squizzato et al., 2013), in Germany (Poulain et al., 2011), and in Singapore (Behera et al., 2013a), thus, extensive research has been performed to study the characteristics of $iPM_{2.5}$ and precursor gases under different atmospheric chemical climatology. In the troposphere, NH_3 gas preferentially reacts with H_2SO_4 to form ammonium sulfate ($(NH_4)_2SO_4$) and ammonium bisulfate (NH_4HSO_4) (Seinfeld and Pandis, 2006). If excessive NH_3 is available,

* Corresponding author.
E-mail address: lwang5@ncsu.edu (L. Wang-Li).

https://doi.org/10.1016/j.atmosres.2020.105190
Received 16 April 2020; Received in revised form 22 June 2020; Accepted 6 August 2020
Available online 11 August 2020

ammonium nitrate (NH_4NO_3) salt is expected to exist in $iPM_{2.5}$; however, the fractional contribution of NH_4NO_3 to $iPM_{2.5}$ depends on environmental conditions (Nenes et al., 1998; Pathak et al., 2009). Due to its lack of thermal stability, NH_4NO_3 may decompose to the gaseous form of HNO_3 and NH_3 under high temperature (T) and low relative humidity (RH), the environmental conditions that do not favor the particle phase. On the other hand, sulfate (SO_4^{2-}) salts are relatively thermally stable compared with nitrate (NO_3^-) salts and the vapor pressure of H_2SO_4 is very low, thus, almost all the NH_3 that reacted with SO_4^{2-}stays in the particle phase (Olszyna et al., 2005; Seinfeld and Pandis, 2006). Moreover, nonvolatile cations such as sodium (Na^+), calcium (Ca^{2+}), magnesium (Mg^{2+}), and potassium (K^+) may also exist in $iPM_{2.5}$ and coarse particles and poses great influence on the partitioning of NH_3–NH_4^+ (Anlauf et al., 2006; Makar et al., 1998; Snider et al., 2016).

In the atmospheric boundary layer, the gas-phase NH_3 is directly emitted from emission sources (Meng et al., 2018; Reche et al., 2015), while HNO_3 and H_2SO_4 are largely transformed from gaseous pollutants such as nitrogen oxides (NO_x) (NO_x = NO + NO_2) and sulfur dioxide (SO_2) through (photo)chemical reactions (Behera et al., 2013b; Khoder, 2002; USEPA, 2019; Wang et al., 2006). The major NH_3 emission sources include agriculture, industrial processes, automobile emissions, soil, and oceans (Behera et al., 2013b; Pan et al., 2016). Whaley et al. (2018) noted the important role of bidirectional flux of NH_3 on ambient NH_3 levels. And NH_3 emissions from agricultural sources such as animal feeding operations (AFOs) are the largest sources of atmospheric NH_3 in the U.S. (USEPA, 2004; McQuilling, 2016). Thus, the AFOs NH_3 emissions may have important impact on the atmospheric chemistry of secondary $iPM_{2.5}$ (Stokstad, 2014; Wang-Li, 2015; Cheng, 2018) and research has indicated that NH_3 has substantial influence on $PM_{2.5}$ pH, the increase of NH_3 gas concentrations may lead to the decrease of particle pH under NH_3-rich conditions (Song et al., 2018). Once emitted, NH_3 will experience complex transport and transformation processes prior to its removal (see Fig. 1).

Tropospheric lifetime of NH_3 is from 0.5 h to 5 d (Seinfeld and Pandis, 2006) with dry deposition being the major removal process (Walker et al., 2019). Due to its short lifetime, the spatial variation of atmospheric concentration of NH_3 can be caused by the variabilities in the emission sources (associated with agricultural activities and presence of AFOs), bidirectional flux of NH_3 (Whaley et al., 2018), and dry deposition rates (associated with the land use practices) (Duyzer, 1994; Phillips et al., 2004; Rattray and Sievering, 2001; Sutton et al., 1994). Due to relatively short lifetime of NH_3 and spatial separation of emission sources of NH_3 and acidic precursor gases (transportation and industrial activities), NH_3 emissions from AFOs may have variable potential for the formation of $iPM_{2.5}$ in rural and urban environments (Cheng, 2018).

In the literature, four chemical parameters have been proposed to evaluate the potential effects of NH_3 emissions on $iPM_{2.5}$ formation (Ansari and Pandis, 1998; Dong et al., 2014; Makar et al., 2009).

First is the gas ratio (GR), which is used to characterize the neutralization degree of NH_3 (Ansari and Pandis, 1998; Dong et al., 2014):

$$GR = \frac{[TA] - 2[TS]}{[TN]} \quad (1)$$

where TA (in units of μmole m^{-3}) equals to the sum of gas-phase NH_3 and aerosol-phase ammonium (NH_4^+), TS (in units of μmole m^{-3}) stands for the total sulfate including SO_4^{2-}, bisulfate (HSO_4^-) and H_2SO_4, and TN (in units of μmole m^{-3}) stands for total amount of NO_3^- and HNO_3. The GR represents the potential for neutralization. If one assumes uniform mixing conditions, GR = 1 would be indicative of full neutralization; GR > 1 would indicate the NH_3-rich condition when all acidic species are fully neutralized and there is excessive NH_3, while GR < 1 would reveal the NH_3-poor condition when acidic species are not fully neutralized. More specifically, atmospheric conditions when 0 < GR < 1 would indicate that the amount of total available NH_3 (gaseous NH_3 + aerosolNH_4^+) is enough to fully neutralize all H_2SO_4, but not total available HNO_3 (gaseous HNO_3 + aerosolNO_3^-). Conditions with GR < 0 would reveal that the amount of total available NH_3 is not enough to fully neutralize either total available H_2SO_4 or total available HNO_3.

Second, gas-phase NH_3 to NH_x ($=NH_3+NH_4^+$) molar fraction can be used to assess the changes in the partitioning of NH_3–NH_4^+(Ellis et al., 2011; Saylor et al., 2015):

$$NH_3/NH_x = \frac{[NH_3]}{[NH_3] + [NH_4^+]} \quad (2)$$

The NH_3/NH_x ratios close to zero would correspond to the conditions when all NH_3 is neutralized by acidic trace gases, while values greater than 0 would describe chemical conditions with excessive unneutralized NH_3 in the gas phase, e.g., the ratio NH_3/NH_x = 0.5, would indicate equal amounts of NH_3 in the gas phase andNH_4^+in the particle phase.

Third, the total available NH_3 to SO_4^{2-}molar ratio (TA/TS) can be used to assess the atmospheric acidic conditions and the possible chemical composition of $iPM_{2.5}$. When TA/TS < 1, both NH_4HSO_4 and H_2SO_4 may exist in inorganic aerosols. When 1 < TA/TS < 2, the NH_4^+ salts in inorganic aerosols may consist of NH_4HSO_4, letovicite

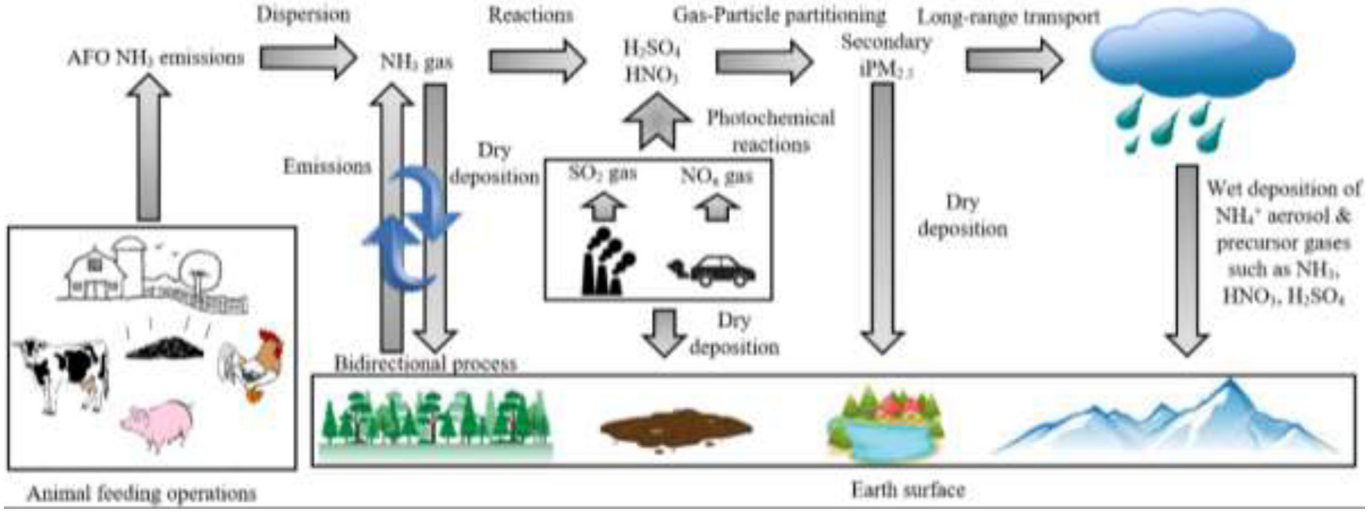

Fig. 1. Fate and transport of NH_3 emitted from AFOs in the atmosphere.

($(NH_4)_3H(SO_4)_2$), and $(NH_4)_2SO_4$. When TA/TS > 2, the NH_4^+ salts in inorganic aerosols may consist of both $(NH_4)_2SO_4$ and NH_4NO_3 (Makar et al., 2009).

$$TA/TS = \frac{[NH_3] + [NH_4^+]}{[SO_4^{2-}]} \quad (3)$$

Fourth, the mass ratio of $NH_4^+ + NO_3^-$ to total $PM_{2.5}$ ($AN/PM_{2.5}$) characterizes the fraction of $PM_{2.5}$ mass that is directly sensitive to the changes in NH_3 emissions. The change of NH_3 emissions is apt to directly affect the concentrations of existing particle NH_4^+ and particleNO_3^- prior to affecting particle SO_4^{2-} (Makar et al., 2009).

$$AN/PM_{2.5} = \frac{NH_4^+ + NO_3^-}{PM_{2.5}} \quad (4)$$

The effects of NH_3 emissions on $iPM_{2.5}$ formation may vary in spatiotemporal scales due to the fate and transport of precursor gases as well as the future climate change and the more stringent regulation rules for pollutants emissions (Cheng et al., 2019). Therefore, more efforts should focus on the investigation of dynamic changes of atmospheric chemical conditions in response to the changes of emissions scenarios. The objective of this study was to investigate the spatial and temporal variations of GR, NH_3/NH_x, TA/TS, and $AN/PM_{2.5}$ in urban and rural areas of the Southeastern U.S. Section 2 describes the study methodology, Section 3 includes the data analysis and discussions, the conclusions are summarized in Section 4.

2. Methodology

2.1. Data collection sites

The data collected at eight Southeastern Aerosol Research and Characterization Network (SEARCH) sites from 2004 to 2016 were used in this study. SEARCH was established in the early 90s to help states monitor $PM_{2.5}$ for regulatory purposes, to collect long-term data for air quality model evaluation, and to identify the long-term spatial and temporal trends of $PM_{2.5}$, mercury (Hg) and ozone (O_3) (USGS, 2016).

As shown in Fig. 2, the SEARCH Network monitored air quality data at eight sites representing urban and rural environments. The details regarding the site description can be found in Hansen et al. (2003) and Blanchard et al. (2013). Briefly, the JST site is an urban site in the midtown of Atlanta. The site is affected by the emissions from local traffic and industrial sources. The YRK site represents a rural site located in a forest and agricultural area of Georgia and is influenced by the emissions from a cattle pasture as well as animal production house emissions. The BHM site is in the city of Birmingham and is impacted by the emissions from traffic and industrial sources. The CTR site is in a forest area approximately 85 km to the southwest of Birmingham and 50 km to the south of Tuscaloosa and is impacted by air masses coming from these two urban areas. The GFP site is an urban site located in coastal area, 1.5 km from the Gulf of Mexico. The atmospheric chemical condition at the GFP site is influenced by residential emission sources, local roads and highways. The OAK site is a rural site located in a forest area, away from industrial emission sources, with AFOs farms located to the north and west of the site. The PNS site is an urban site located in the coastal area, 5 km from the Gulf of Mexico, and is impacted by emission sources coming from industrial activities and major highways. The OLF site is a suburban site, impacted by the nearby residential emissions and local roads. Measurements at all onsite monitoring stations started in 1998/1999. Measurement details at the eight sites are summarized in Table 1.

Table 1
Field measurements at the eight sites.

Observables	Technique	Max resolution	Detection limit
• Gases: ppb			
NO	CL	1–min	0.05
NO_2	Photolysis/CL	1–min	0.1
HNO_3	Denuder/Mo reduction/CL	1–min	0.1
NO_y	Mo reduction/CL	1–min	0.1
SO_2	UV–fluorescence	1–min	0.2
NH_3	Denuder/Pt oxidation/CL	5–min	0.2
• $iPM_{2.5}$ chemical compositions: μg m^{-3}			
SO_4^{2-}	Fe reduction/UV–fluorescence	5–min	0.4
NO_3^-	Filter/Mo reduction/CL	5–min	0.2
NH_4^+	Filter/Pt oxidation/CL	5–min	0.1
• Meteorological conditions:			
T/RH/SR/BP	Various	1–min	N/A
WS/WD/Precipitation	Various	1–min	N/A

CL: chemiluminescence; SR: solar radiation; BP: barometric pressure; WS: wind speed; WD: wind direction; N/A: not applicable.

Concentrations of gas-phase pollutants (e.g., NH_3, HNO_3, SO_2) and $iPM_{2.5}$ chemical compositions (e.g.,NO_3^-,NH_4^+ and SO_4^{2-}) were simultaneously measured using continuous/semi-continuous methods (averaged over 1 h) and filter–based method (averaged over 24 h, not shown in Table 1). Measurement method, duration, frequency, quality control (QC), and quality assurance (QA) were reported by Edgerton et al. (2005, 2006, 2007).

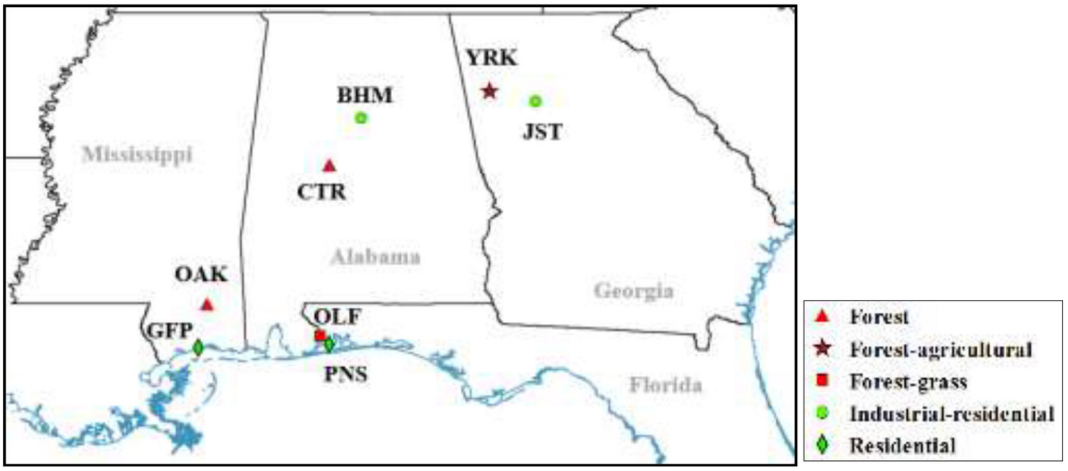

Fig. 2. The geographical locations of the eight monitoring sites under the SEARCH (Green label indicates urban sites; red label indicates rural or suburban sites).

2.2. Data analysis

The following steps were taken to pre-process the 1-h and 24-h average data for the analysis of spatiotemporal variations of GR, NH_3/NH_x, TA/TS, and $AN/PM_{2.5}$:

- Some measurement values were reported to be either negative or below the detection limit (DL) of the instruments. The negative values less than (−DL) were considered questionable and excluded from the dataset, while the other values below the DL were replaced with half of the DL (USEPA, 2000).
- Following the method by Blanchard et al. (2012), the days at each site with more than 3-h precipitation were labeled as wet days and were excluded from the data analysis.
- Following the method by Saylor et al. (2010), the values of each parameter within 10° wind direction bin were grouped together. Average values and 95% confidence intervals of the hourly data in each 10° wind direction were calculated for each wind sector.

The hourly data of NH_3 gas concentration are only available at six out of eight sites and only during specific years: YRK (2008–2016), JST (2010–2016), CTR (2012–2016), BHM (2011–2016), OLF (2013–2016), and OAK (2010). The hourly NH_3 concentrations in 2013 had better data completeness, thus, the investigation of spatial variation of parameters requiring hourly NH_3 gas concentration measurements (i.e., GR, NH_3/NH_x, and TA/TS) was only performed at the YRK, JST, CTR, BHM, and OLF sites in 2013 and at the OAK site in 2010. The temporal variation of NH_3/NH_x, TA/TS, $AN/PM_{2.5}$ at eight sites was based on 24-h average filter-based data in 2004–2013 and 1-h average data in 2014–2016 due to the change of monitoring practice. Diurnal and seasonal variations of $AN/PM_{2.5}$ at six sites were based on 1-h average data. As for YRK, JST, CTR, BHM, and OLF sites, the completeness of hourly $AN/PM_{2.5}$ data is better in 2013, thus, the data in 2013 at these sites were chosen for diurnal and seasonal analysis. While as for OAK site, the hourly $AN/PM_{2.5}$ data were only available in 2010, thus, the diurnal and seasonal analysis of $AN/PM_{2.5}$ was only performed in 2010 at the OAK site. Tukey honest significant difference (HSD) test was utilized to check the year-to-year temporal variation of NH_3/NH_x, TA/TS, and $AN/PM_{2.5}$.

To obtain thorough information of AFOs distribution, visual check of the zoom-in Google map approach was used to identify the dry-based poultry farms and wet-based swine farms locations. Spatial distribution of the poultry and swine farms within 100 km (radius) of the eight sites was used to assist wind sector analysis.

3. Results and discussion

3.1. Spatial variation of the GRs

Fig. 3 shows the wind sector analysis of GR values at the six sites. According to Fig. 3, as for YRK and JST sites, GR values were greater than one, suggesting NH_3-rich conditions at these two sites for all wind directions. In terms of the BHM and CTR sites, the BHM site exhibited NH_3-rich conditions with the GRs greater than one for all wind directions; while for the CTR site, GR values varied in different wind directions with GR values greater than one for the southeasterly and westerly wind directions. The OLF site was in NH_3-rich area with GRs greater than one for all wind directions, while the GRs at the OAK site exhibited variations in different wind directions with GR values greater than one for the westerly-northwesterly wind directions.

Out of all the sites examined, Fig. 3 shows that the largest GR values occurred at the YRK site in the wind direction of 100°-130°. The YRK site also exhibited large variations in GRs for different wind directions, suggesting the possibility of significant NH_3 emission sources at the proximity of the site. The Google map (see Fig. 4) shows three poultry farms located at 1.5 km, 1.5 km, and 3.1 km southeast (100°-130°) of the YRK site. This result is consistent with the findings of Saylor et al. (2010) who analyzed the NH_3 gas and NH_x concentrations for different wind directions at the YRK site in 2007 and reported significantly higher NH_3 gas and NH_x concentrations in the wind direction of 100°-140°. The wind direction-based analysis of GRs reveals that AFOs farms, located in the distance of 1.5–3.1 km upwind, can significantly affect the GR values at the YRK site. The continuous hourly measurements captured the dynamic variation of different gas-phase and particle phase pollutants at the YRK site, the event with high NH_3 concentration was detected at the YRK site on November 3–5, 2013 (Fig. S1), which confirmed the influences from NH_3 emissions of AFOs farms.

In addition, Fig. 3 shows some dependence of GRs on the wind direction at the JST site. Blanchard et al. (2012) used chemical mass balance (CMB) method and U.S. EPA's National Emission Inventory (NEI) to estimate the contributions of various emission sources to the gas-phase and particle-phase pollutants in the Southeastern U.S. Their results indicated that at the JST site, vehicle emissions contributed to the largest portion of NH_x concentration. It is believed that NH_3 emissions from a trucking facility (located within 100 m to the north of the JST site) and a parking lot (located within 150 m to the east of the JST site) may be responsible for higher GR values in 10°-20° and 70°-100° sectors, respectively (Google map check). Moreover, a rail yard, a wastewater treatment facility, and a power plant located within 3.6 km to 7.5 km to the northwest of the JST site could be responsible for NH_3 emissions, causing higher values of GRs in 310°-340° wind directions (Fig. S2).

Fig. 3 shows that the GRs exhibited higher values in the wind direction of 30°-50° at the BHM site. Three large industrial emissions sources were located to the northeast of the BHM site (USEPA, 2011); the Google map in 2016 also confirmed the existence of these three large industrial emissions sources. To the northeast of the BHM site, one steel mills as well as ferroalloy manufacturing plant are 4.6 km away from the BHM site, the coke battery plants in these facilities are important emission sources of NH_3, SO_2, and NO_x. In addition, one construction material company is 3.4 km away from the BHM site; crushed limestone mining and quarrying emitted both SO_2 and NO_x. And calcium carbonate ($CaCO_3$) from limestone may also compete with NH_3 to react with available HNO_3. The closest industrial source to the northeast of the BHM site is an iron foundry company, the coke battery in the company emitted NH_3, SO_2, and NO_x (Fig. S3).

At the CTR site, the NH_3-poor conditions dominated in 2013; while in the wind direction of 140°-170°, the GRs were greater than two. The NH_x concentration vs. wind direction at the CTR site didn't exhibit the higher NH_x concentration to the southeast of the CTR site, therefore, the higher GRs in the wind direction of 140°-170° may be due to the lack of acidic gases, the lower acidic gases (HNO_3 and H_2SO_4) concentrations in the wind direction of 140°-170° still led to higher GRs.

The GRs exhibits higher values to the west and northeast of the OLF site. The NH_x concentration vs. wind direction analysis indicates that the higher NH_x concentration appeared to the west and northeast of the OLF site as well. The geographic location of the OLF site may explain the variations of NH_x concentration and GRs in different wind directions. The forest and grassland are located to the north and south of the OLF site, therefore, lack of NH_3 emission sources in these two wind directions leads to lower NH_x concentration and GRs.

As for the OAK site, higher GRs appear in the wind direction of 200°-220° and 280°-350°, this may be explained by the AFOs NH_3 emissions surrounding the OAK site. The AFOs farms distribution within 100 km of the paired sites-OAK and PNS sites is in Fig. 5.

The OAK site is about 67 km to the Gulf of Mexico in the coastal area. Moreover, the OAK site is in the forest area with a large number of AFOs farms located to the north and west of the site. The source apportionment analysis by Blanchard et al. (2012) showed that agricultural NH_3 contributed to more than half of the NH_x concentration at the OAK site. The forest may have higher deposition rates and inhibit the transport of NH_3, SO_2, and NO_x to the OAK site from the southerly

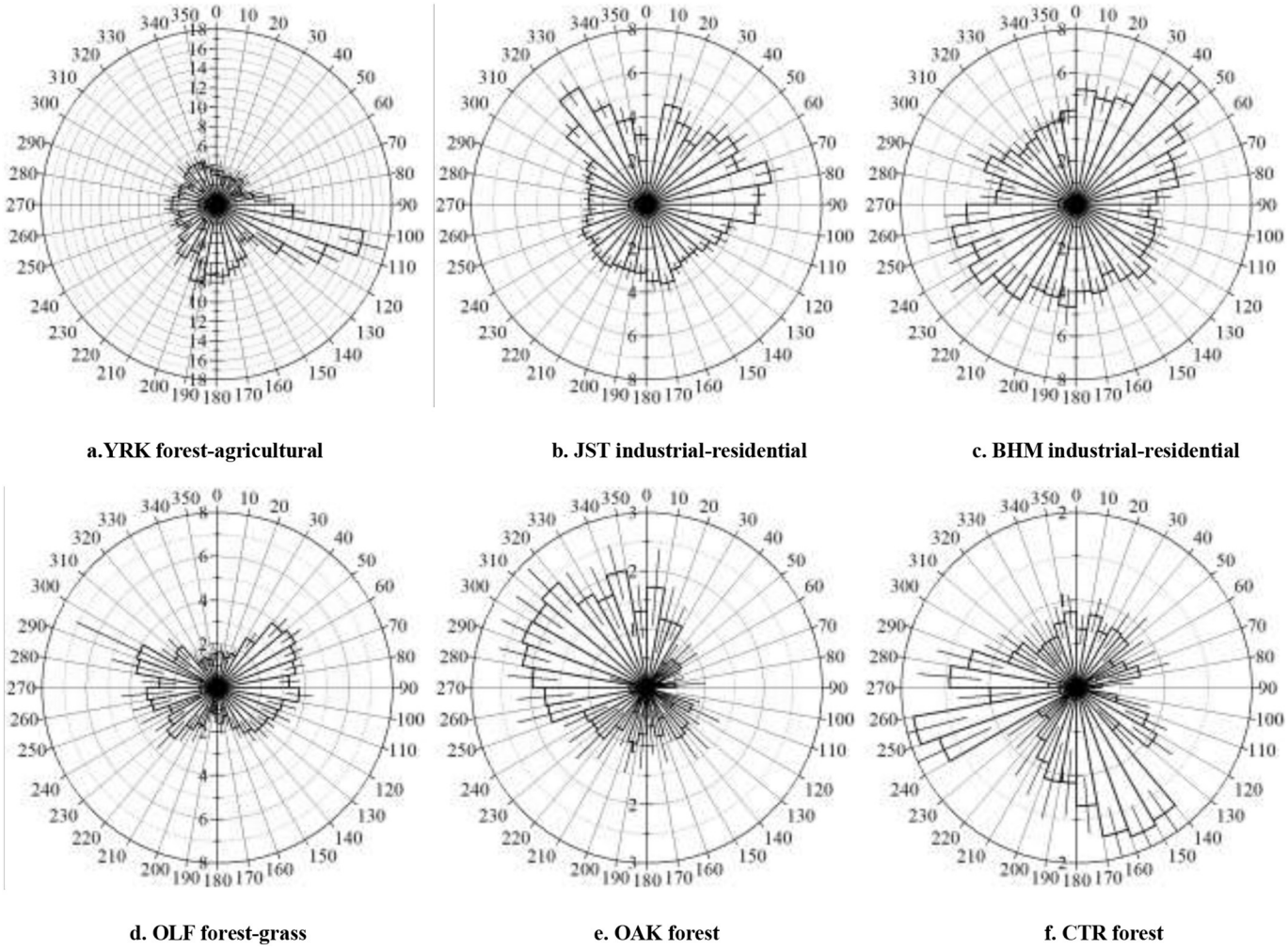

Fig. 3. The GRs at the YRK, JST, CTR, BHM, and OLF sites in 2013 and OAK site in 2010 (Note different scales in the figures).

and easterly wind directions, while the significant NH_3 emissions from AFOs farms to the north of the OAK site may pose great impact on the GR, thus making the GRs higher in northwesterly wind direction at the OAK site.

3.2. Spatial and temporal variations of NH_3/NH_x

The change of NH_3–NH_4^+ partitioning in response to changes of the precursor gas emissions can be characterized by gas-phase NH_3 molar fraction (i.e. NH_3/NH_x). Out of all the sites examined in this study,

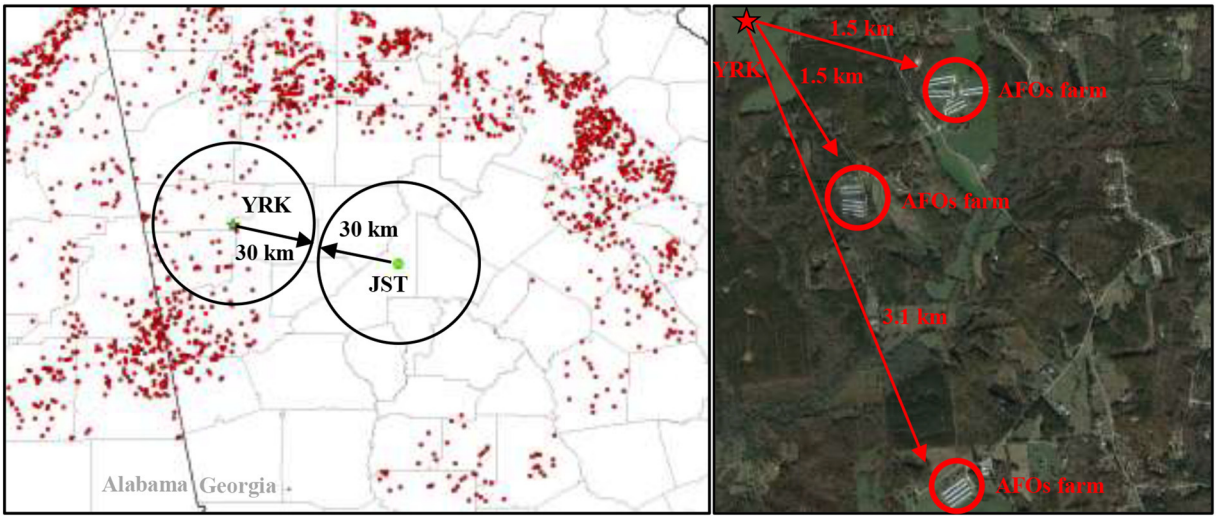

Fig. 4. AFOs farm distribution within 100 km of the YRK and JST sites (left) and in the proximity of the YRK site (right).

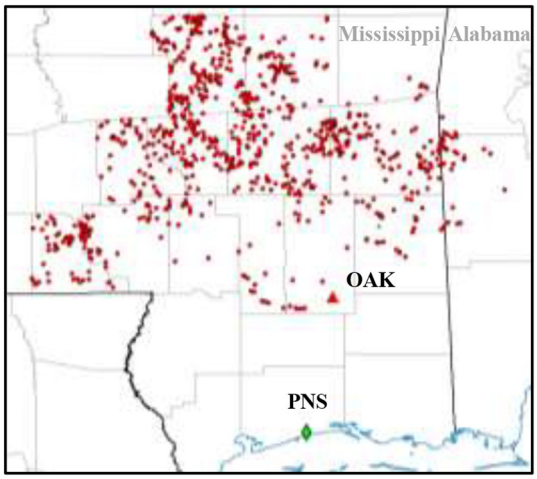

Fig. 5. AFOs farm distribution within 100 km of the OAK and PNS sites.

NH_3/NH_x exhibited a significantly upward trend over the past 13 years, with the exception of BHM and PNS sites (see Table 2). This upward trend is consistent with the analysis of Saylor et al. (2015). The observed increase in NH_3/NH_x indicates that both increase in NH_3 concentrations and the reduction in acidic precursor gases concentrations (NO_x & SO_2) rendered the partitioning of NH_3–NH_4^+ toward gas phase, thus, the formation of $iPM_{2.5}$ tended to be limited by the availability of acidic gases instead of NH_3. Xing et al. (2013) noted the decreasing trend in NO_x and SO_2 emissions due to the implementation of various regulations such as clean air interstate rule (CAIR) in 2005 and cross-state air pollution rule (CSAPR) in 2011.

Fig. 6 shows the NH_3/NH_x ratios under different wind directions at the six sites. According to Fig. 6, an excessive amount of NH_3 in the gas phase was measured at all the sites. The NH_3/NH_x ratio was higher (more than 60% of NH_x was in the gas phase) at YRK, JST, and BHM sites compared to OAK, OLF, and CTR sites (where ~40% of the NH_x resided in the gas phase). The variation of the NH_3/NH_x in different wind directions can be explained by the spatial heterogeneity of the $iPM_{2.5}$ precursor gas emission sources as well as the fate and transport of various precursor gases (Fine et al., 2008; Wang-Li, 2015). At the YRK site, the NH_3/NH_x was higher in the wind direction of 100°-120°, which can be attributed to NH_3 emissions from the AFOs located southeast of the YRK site (see Fig. 4). At the OAK site, the NH_3/NH_x ratios were generally higher for the air masses coming from the westerly-northwesterly directions, which may also be explained by the NH_3 emissions from AFOs farms. The fate and transport of precursor gases contributed to the variation of NH_3/NH_x ratios in different wind directions at each site, and the wind-direction dependence of NH_3/NH_x ratios provided important information for the partitioning of NH_3-NH_4^+ due to spatial distribution of precursor gases sources.

3.3. Spatial and temporal variations of TA/TS

The yearly averaged values of TA/TS for 2004–2016 are summarized in Table 3. According to Table 3, the TA/TS exhibits a significantly upward trend at the eight sites. The upward trend in TA/TS was associated with the reduction in SO_2 emissions and increase in NH_3 emissions in the Southeastern U.S. Less SO_2 was available to be transformed into H_2SO_4 through (photo)chemical reactions, leading to lower concentration ofSO_4^{2-} in the particle phase (Xing et al., 2013). Overall, Table 3 shows that the annual average values of TA/TS at the eight sites (except OAK site in 2004) were greater than 2 in the past 13 years, indicating that NH_4^+ salts in inorganic aerosols may consist of both $(NH_4)_2SO_4$ and NH_4NO_3.

The TA/TS under different wind directions at the six sites are shown in Fig. 7. For the spatial variation, TA/TS exhibited lower values at the OLF, OAK, and CTR sites, higher values at the YRK, JST and BHM sites. The agricultural NH_3 emission sources at the YRK site, NH_3 emissions from vehicles at the JST and BHM sites might have made the TA/TS higher. Especially in the wind direction of 100°-130° at the YRK site, the values of TA/TS were significantly higher than the other wind directions, which indicates the impact of poultry farm NH_3 emissions to the southeast of the YRK site.

3.4. Spatial and temproal variations of $AN/PM_{2.5}$

The temporal variation of $AN/PM_{2.5}$ at the eight sites in 2004–2016 is shown in Table 4. The $AN/PM_{2.5}$ values at YRK, JST, CTR, and OLF sites exhibited a significantly downward trend over the past 13 years. Saylor et al. (2015) analyzed the temporal variation of NH_4^+ andNO_3^- in the Southeastern U.S. in 2004–2012 and discovered a significant reduction trend at the eight sites. The reduction in the sum concentrations of NH_4^+ and NO_3^- may result in the reduction of $AN/PM_{2.5}$, and the NO_3^- can also switch to coarse mode due to the presence of base cations, which may also led to the reduction of $AN/PM_{2.5}$. Thus, smaller fraction of $PM_{2.5}$ mass was directly NH_3 sensitive.

The diurnal and seasonal variations of $AN/PM_{2.5}$ at six sites were analyzed and are shown in Fig. 8. As it can be seen, $AN/PM_{2.5}$ exhibited a significantly seasonal and diurnal pattern at six sites. For seasonal variation, the values of $AN/PM_{2.5}$ were higher in colder seasons and lower in hotter seasons. The semi-volatile characteristic of NH_4NO_3 can explain the seasonal variation (Olszyna et al., 2005; Poulain et al., 2011). The NH_4NO_3 aerosol is not thermally stable under high T such as summer conditions, thus, NH_4NO_3 decomposes into gas-phase NH_3 and HNO_3; while under low T such as winter conditions, NH_4NO_3 tends to stay in particle phase. For diurnal variation, the values of $AN/PM_{2.5}$

Table 2
Yearly averaged values of NH_3/NH_x at the eight sites.

Year	YRK	JST	BHM	CTR	GFP	OAK	PNS	OLF
2004	0.45 ± 0.21	0.40 ± 0.19	0.54 ± 0.20	0.17 ± 0.13	0.36 ± 0.21	0.18 ± 0.13	0.41 ± 0.21	0.27 ± 0.16
2005	0.49 ± 0.19	0.42 ± 0.18	0.57 ± 0.19	0.19 ± 0.15	0.38 ± 0.20	0.22 ± 0.15	0.39 ± 0.18	0.28 ± 0.17
2006	0.53 ± 0.18	0.39 ± 0.17	0.55 ± 0.17	0.18 ± 0.12	0.42 ± 0.20	0.23 ± 0.16	0.39 ± 0.18	0.27 ± 0.15
2007	0.61 ± 0.17	0.48 ± 0.17	0.58 ± 0.17	0.29 ± 0.21	0.44 ± 0.18	0.25 ± 0.18	0.44 ± 0.19	0.31 ± 0.16
2008	0.53 ± 0.20	0.44 ± 0.15	0.61 ± 0.15	0.18 ± 0.12	0.40 ± 0.18	0.19 ± 0.15	0.38 ± 0.19	0.26 ± 0.16
2009	0.61 ± 0.18	0.53 ± 0.16	0.60 ± 0.16	0.24 ± 0.15	0.45 ± 0.17	0.25 ± 0.14	0.42 ± 0.17	0.31 ± 0.15
2010	0.59 ± 0.19	0.51 ± 0.15	0.60 ± 0.13	0.23 ± 0.14	0.45 ± 0.18	0.26 ± 0.16	N/A	0.30 ± 0.20
2011	0.58 ± 0.17	0.56 ± 0.16	0.57 ± 0.17	0.26 ± 0.16	0.43 ± 0.17	N/A	N/A	0.31 ± 0.15
2012	0.69 ± 0.14	0.62 ± 0.14	0.62 ± 0.15	0.28 ± 0.13	0.48 ± 0.17	N/A	N/A	0.35 ± 0.15
2013	0.59 ± 0.18	0.62 ± 0.16	0.57 ± 0.17	0.28 ± 0.15	N/A	N/A	N/A	0.36 ± 0.14
2014	0.58 ± 0.14	0.63 ± 0.14	0.56 ± 0.15	0.32 ± 0.13	N/A	N/A	N/A	0.37 ± 0.14
2015	0.62 ± 0.17	0.66 ± 0.16	0.48 ± 0.17	0.35 ± 0.17	N/A	N/A	N/A	0.44 ± 0.13
2016	N/A	0.66 ± 0.14	N/A	0.34 ± 0.15	N/A	N/A	N/A	N/A

N/A: Not available.

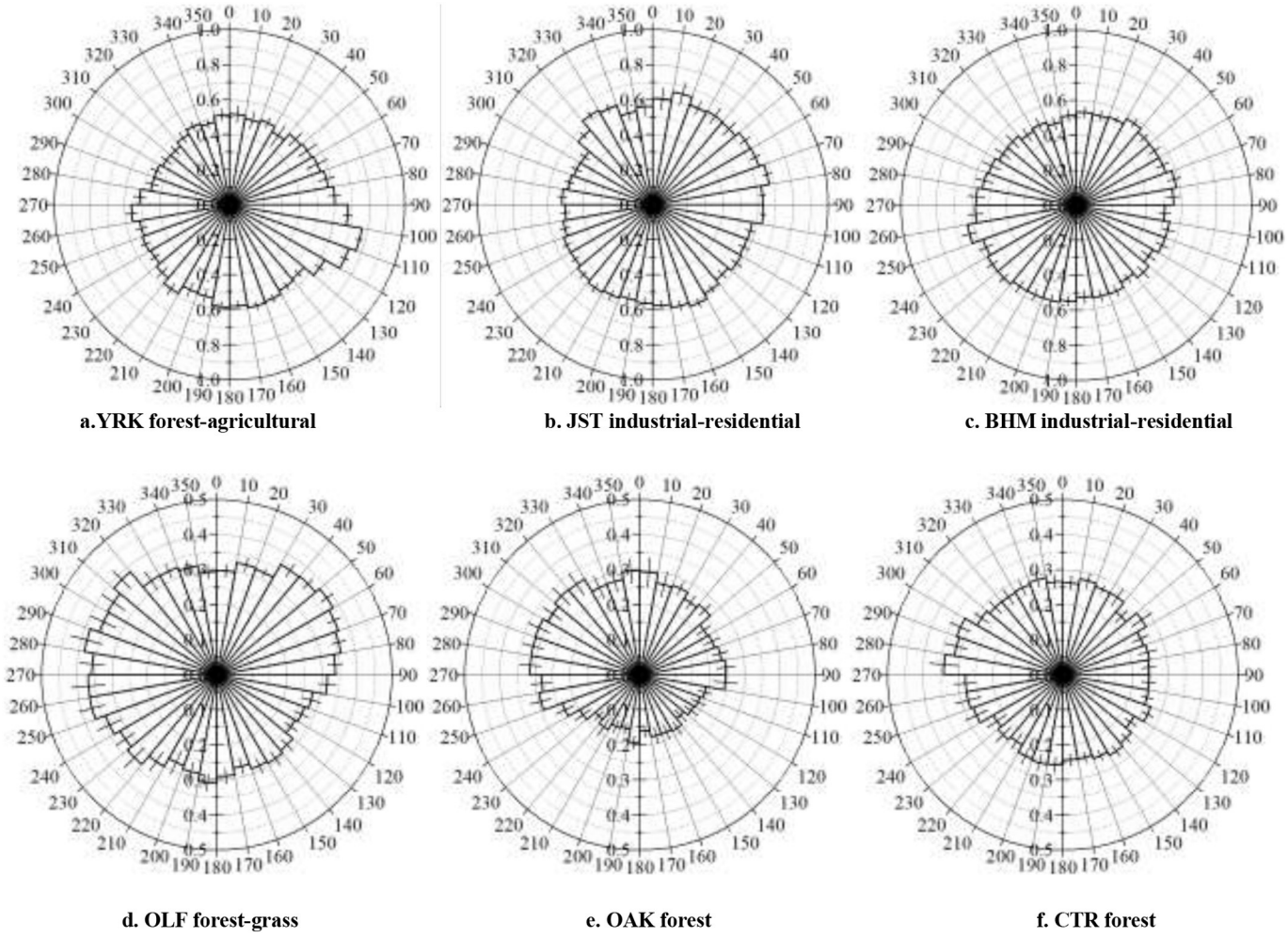

Fig. 6. The NH_3/NH_x under various wind direction at the YRK, JST, CTR, BHM, and OLF sites in 2013 and OAK in 2010. Note different scales on figures.

Table 3
Yearly averaged values of the TA/TS at the eight sites.

Year	YRK	JST	BHM	CTR	GFP	OAK	PNS	OLF
2004	4.32 ± 3.00	3.53 ± 1.60	4.53 ± 2.44	2.09 ± 0.62	2.72 ± 1.25	1.92 ± 0.71	3.09 ± 1.51	2.26 ± 0.74
2005	4.70 ± 3.00	3.77 ± 1.75	4.78 ± 2.74	2.17 ± 0.99	3.01 ± 2.05	2.12 ± 1.12	2.97 ± 1.15	2.52 ± 1.42
2006	5.20 ± 4.50	3.49 ± 1.44	4.52 ± 1.97	2.05 ± 0.60	3.05 ± 1.50	2.18 ± 1.24	2.91 ± 1.11	2.28 ± 0.68
2007	7.85 ± 9.39	4.34 ± 1.92	5.27 ± 3.22	3.00 ± 2.87	3.21 ± 1.93	2.29 ± 1.28	3.48 ± 2.00	2.66 ± 0.88
2008	6.08 ± 4.26	3.95 ± 1.76	5.62 ± 3.74	2.44 ± 1.24	3.11 ± 1.40	2.29 ± 0.93	3.00 ± 1.20	2.51 ± 1.17
2009	6.94 ± 4.45	4.86 ± 2.00	5.91 ± 6.67	2.66 ± 1.04	3.75 ± 2.18	2.41 ± 0.98	3.54 ± 1.56	2.64 ± 0.94
2010	6.30 ± 3.62	4.62 ± 1.61	5.31 ± 1.85	2.47 ± 0.74	3.74 ± 2.14	2.60 ± 0.94	N/A	2.98 ± 1.46
2011	6.16 ± 4.08	5.30 ± 2.58	5.51 ± 2.78	2.66 ± 0.97	3.55 ± 1.49	N/A	N/A	2.96 ± 0.92
2012	7.94 ± 4.37	5.95 ± 2.71	5.81 ± 2.54	2.55 ± 0.86	3.78 ± 2.34	N/A	N/A	3.11 ± 1.62
2013	6.20 ± 3.58	6.52 ± 3.64	5.50 ± 2.71	2.61 ± 0.72	N/A	N/A	N/A	2.98 ± 0.76
2014	9.30 ± 7.52	8.00 ± 4.42	7.76 ± 5.28	4.63 ± 3.89	N/A	N/A	N/A	4.09 ± 2.39
2015	18.59 ± 15.73	12.13 ± 10.11	13.32 ± 10.81	9.43 ± 8.18	N/A	N/A	N/A	9.26 ± 7.82
2016	N/A	14.91 ± 8.72	N/A	9.11 ± 6.25	N/A	N/A	N/A	N/A

N/A: Not available.

were higher at noon. This may be explained by the diurnal variation of $PM_{2.5}$ mass, NH_4^+ and NO_3^- concentrations. Edgerton et al. (2006) analyzed the diurnal variation of $PM_{2.5}$ mass concentration and its chemical compositions at the SEARCH eight sites, the results indicated that the $PM_{2.5}$ mass and NO_3^- concentrations exhibited higher values in the early morning and at night and lower values in the daytime due to the diurnal change of planetary boundary layer (PBL) height and turbulent mixing. While NH_4^+ concentration exhibited no specific diurnal pattern, the combined effects of the diurnal variation of $PM_{2.5}$ mass, NH_4^+ and NO_3^- concentrations leads to the higher $AN/PM_{2.5}$ at noon.

The values of $AN/PM_{2.5}$ were higher at the JST and BHM sites than the YRK and CTR sites at noon. This can be explained by the abundance of the NO_x and SO_2 gas in the urban areas. The NO_x gas emitted from vehicles and SO_2 gas emitted from electricity generating unit (EGU) can be transformed by the more intense solar radiation into HNO_3 and H_2SO_4 at noon at the JST and BHM sites. The NH_3-rich condition at the JST and BHM sites facilitated the reaction of NH_3 with HNO_3 and H_2SO_4.

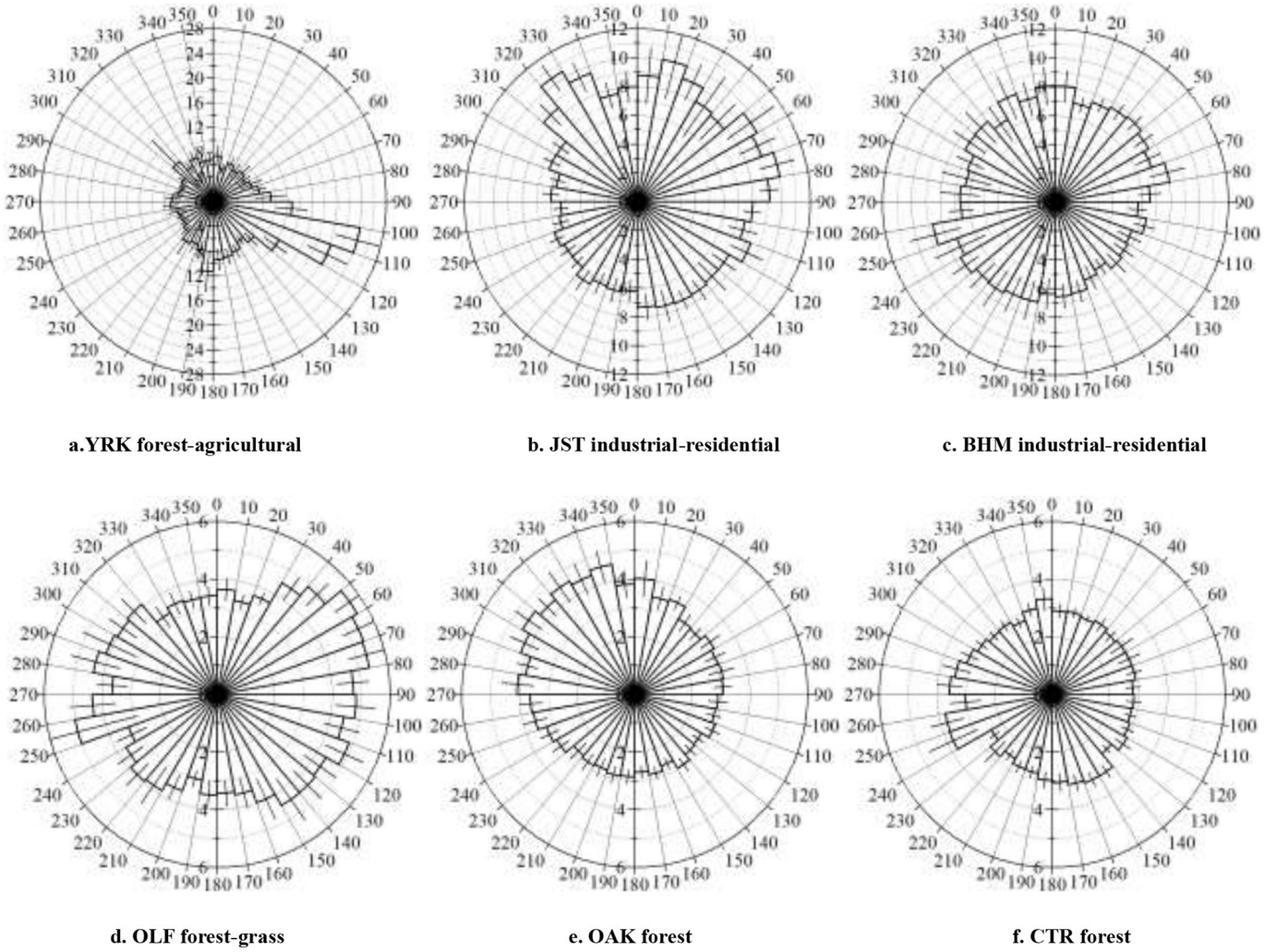

Fig. 7. The TA/TS under different wind direction at the YRK, JST, CTR, BHM, and OLF sites in 2013 and OAK in 2010. Note different scales on figures.

4. Conclusions

Spatial and temporal variations of atmospheric chemical conditions at eight urban/nonurban sites under SEARCH Network were investigated based on the analysis of four parameters, i.e., GR, NH_3/NH_x, TA/TS, and $AN/PM_{2.5}$. It is discovered that from 2004 to 2016, both $(NH_4)_2SO_4$ and NH_4NO_3 existed in $iPM_{2.5}$ at the eight sites. The GRs analysis reveals that AFOs NH_3 emissions contributed to the higher GRs at two rural monitoring sites coded as YRK and OAK in the wind direction coming from AFOs. An upward temporal trend of NH_3/NH_x ratio was observed, indicating relatively more NH_3 stayed in gas phase over the last decade. The TA/TS also exhibited an increase trend in 2004–2016, in response to the reduction in SO_2 emissions in the Southeastern U.S. over the time. The $AN/PM_{2.5}$ analysis indicates that smaller fraction of $PM_{2.5}$ mass was directly NH_3 sensitive over the time span studies here. Understanding of the spatial and temporal variations of atmospheric chemical conditions provides insights to improve our understanding of $iPM_{2.5}$ formation under rural and urban conditions,

Table 4
Yearly averaged values of $AN/PM_{2.5}$ at the eight sites.

Year	YRK	JST	BHM	CTR	GFP	OAK	PNS	OLF
2004	0.16 ± 0.06	0.15 ± 0.06	0.14 ± 0.07	0.13 ± 0.06	0.12 ± 0.04	0.11 ± 0.04	0.11 ± 0.03	0.12 ± 0.03
2005	0.17 ± 0.06	0.16 ± 0.06	0.13 ± 0.06	0.12 ± 0.04	0.13 ± 0.09	0.11 ± 0.04	0.12 ± 0.03	0.13 ± 0.04
2006	0.17 ± 0.08	0.14 ± 0.06	0.13 ± 0.06	0.12 ± 0.06	0.12 ± 0.04	0.11 ± 0.05	0.12 ± 0.04	0.13 ± 0.06
2007	0.19 ± 0.08	0.16 ± 0.07	0.14 ± 0.08	0.12 ± 0.05	0.13 ± 0.05	0.12 ± 0.04	0.12 ± 0.03	0.12 ± 0.03
2008	0.18 ± 0.07	0.17 ± 0.08	0.14 ± 0.07	0.13 ± 0.06	0.13 ± 0.06	0.12 ± 0.04	0.12 ± 0.03	0.13 ± 0.04
2009	0.17 ± 0.08	0.15 ± 0.08	0.14 ± 0.08	0.12 ± 0.06	0.13 ± 0.08	0.11 ± 0.05	0.12 ± 0.04	0.12 ± 0.04
2010	0.17 ± 0.11	0.15 ± 0.08	0.13 ± 0.08	0.12 ± 0.06	0.12 ± 0.04	0.13 ± 0.07	N/A	0.12 ± 0.04
2011	0.15 ± 0.08	0.14 ± 0.08	0.14 ± 0.07	0.13 ± 0.07	0.13 ± 0.06	N/A	N/A	0.13 ± 0.05
2012	0.12 ± 0.06	0.13 ± 0.07	0.11 ± 0.05	0.11 ± 0.04	0.12 ± 0.04	N/A	N/A	0.11 ± 0.03
2013	0.14 ± 0.07	0.14 ± 0.07	0.13 ± 0.08	0.10 ± 0.05	N/A	N/A	N/A	0.11 ± 0.03
2014	0.11 ± 0.08	0.14 ± 0.11	0.13 ± 0.09	0.09 ± 0.05	N/A	N/A	N/A	0.09 ± 0.03
2015	0.13 ± 0.10	0.19 ± 0.14	0.14 ± 0.10	0.08 ± 0.06	N/A	N/A	N/A	0.10 ± 0.04
2016	N/A	0.14 ± 0.11	N/A	0.08 ± 0.04	N/A	N/A	N/A	N/A

N/A: Not available.

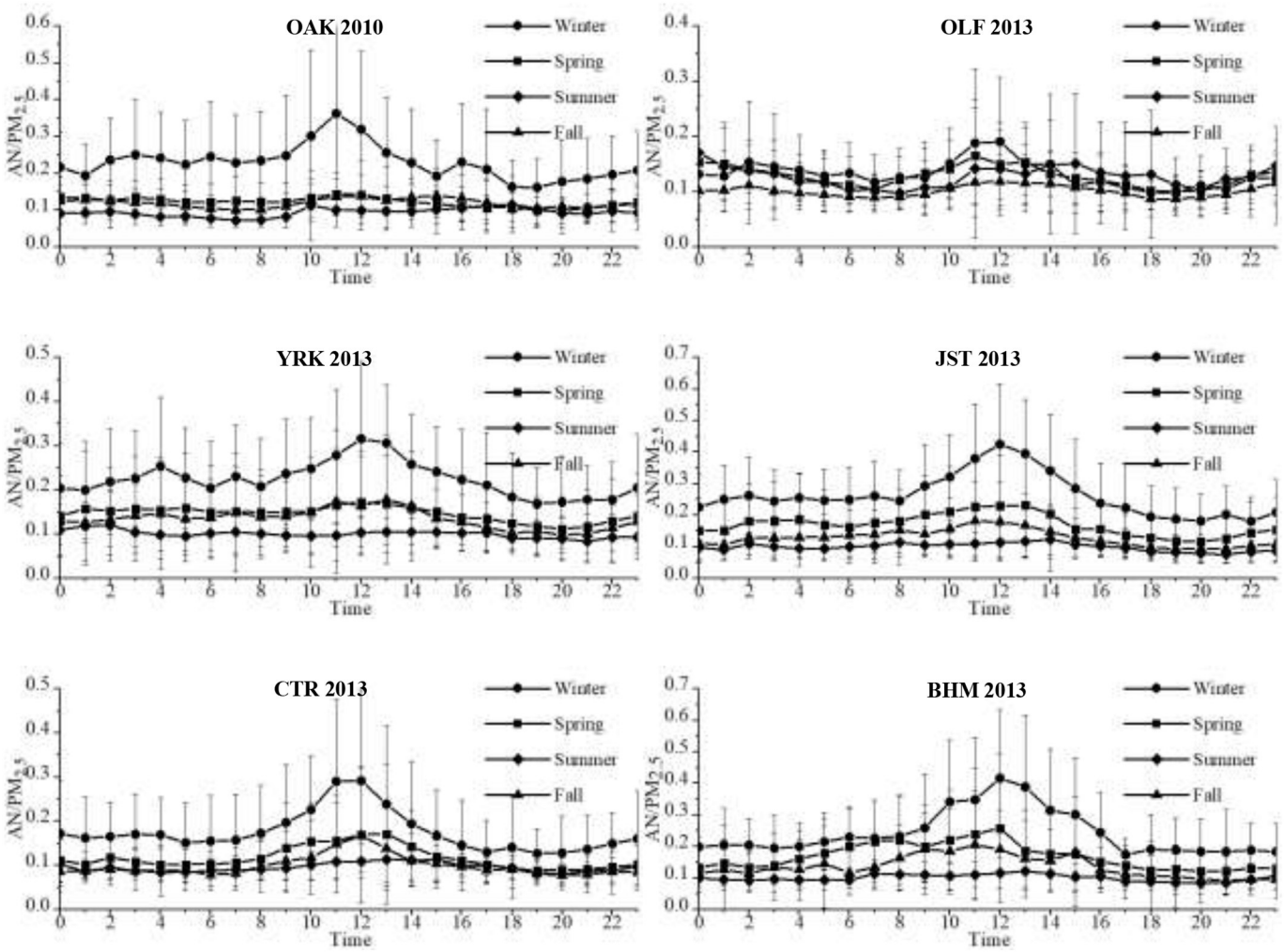

Fig. 8. Diurnal and seasonal variations of the $AN/PM_{2.5}$ at six sites. Note the different scales on figures.

the reduction in SO_2 and NO_x emissions resulted in the reduction of $iPM_{2.5}$ formation despite the increase in NH_3 emissions in the Southeastern U.S..

Author statement

BC and LWL conceived the study; BC performed the data analysis. LWL, as BC's Ph.D. advisor, advised data analysis and interpretation. NM, JC and PB, as BC's Ph.D. committee members, provided assist on data analysis and data interpretation. BC wrote the paper with inputs from all co-authors.

Funding

This project was in part supported by the NSF Award No. CBET-1804720.

Declaration of Competing Interest

None.

Acknowledgements

Great thanks to Eric Edgerton from ARA, Inc. for providing the SEARCH data.

Appendix A. Supplementary data

Supplementary data to this article can be found online at https://doi.org/10.1016/j.atmosres.2020.105190.

References

Anlauf, K., Li, S.M., Leatich, R., Brook, J., Hayden, K., Toom-Sauntry, D., Wiebe, A., 2006. Ionic composition and size characteristics of particles in the lower Fraser Valley: Pacific 2001 field study. Atmos. Environ. 40, 2662–2675.

Ansari, A.S., Pandis, S.N., 1998. Response of inorganic PM to precursor concentrations. Environ. Sci. Technol. 32, 2706–2714.

Behera, S.N., Betha, R., Balasubramanian, R., 2013a. Insights into chemical coupling among acid gases, ammonia and secondary inorganic aerosols. Aerosol Air Qual. Res. 13, 1282–1296.

Behera, S.N., Sharma, M., Aneja, V.P., Balasubramanian, R., 2013b. Ammonia in the atmosphere: a review on emission sources, atmospheric chemistry and deposition on terrestrial bodies. Environ. Sci. Pollut. Res. 20, 8092–8131.

Bell, M.L., Dominici, F., Ebisu, K., Zeger, S.L., Samet, J.M., 2007. Spatial and temporal variation in $PM_{2.5}$ chemical composition in the United States for health effects studies. Environ. Health Perspect. 115, 989–995.

Blanchard, C.L., Tanenbaum, S., Hidy, G.M., 2012. Source contributions to atmospheric gases and particulate matter in the Southeastern United States. Environ. Sci. Technol. 46, 5479–5488.

Blanchard, C.L., Hidy, G.M., Tanenbaum, S., Edgerton, E.S., Hartsell, B.E., 2013. The Southeastern Aerosol Research and Characterization (SEARCH) study: Spatial variations and chemical climatology, 1999–2010. J. Air Waste Manage. Assoc. 63, 260–275.

Cambra-Lopez, M., Aarnink, A.J.A., Zhao, Y., Calvet, S., Torres, A.G., 2010. Airborne particulate matter from livestock production systems: a review of an air pollution problem. Environ. Pollut. 158, 1–17.

Cheng, B., 2018. Dynamics of Rural and Urban Atmospheric Chemical Conditions and

Inorganic Aerosols. Dissertation. North Carolina State University.
Cheng, B., Wang-Li, L., 2019a. Spatial and temporal variations of $PM_{2.5}$ in North Carolina. Aerosol Air Qual. Res. 19, 698–710.
Cheng, B., Wang-Li, L., 2019b. Responses of secondary inorganic $PM_{2.5}$ to precursor gases in an ammonia abundant area in North Carolina. Aerosol Air Qual. Res. 19, 1126–1138.
Cheng, B., Wang-Li, L., Meskhidze, N., Classen, J., Bloomfield, P., 2019. Spatial and temporal variations of $PM_{2.5}$ mass closure and inorganic $PM_{2.5}$ in the Southeastern U.S. Environ. Sci. Pollut. Res. 26, 33181–33319.
Dong, X., Li, J., Fu, J., Gao, Y., Huang, K., Zhuang, G., 2014. Inorganic aerosols responses to emission changes in Yangtze River Delta, China. Sci. Total Environ. 481, 522–532.
Duyzer, J., 1994. Dry deposition of ammonia and ammonium aerosols over heathland. J. Geophys. Res. 99, 18757.
Edgerton, E.S., Hartsell, B.E., Saylor, R.D., Jansen, J.J., Hansen, D.A., Hidy, G.M., 2005. The Southeastern Aerosol Research and Characterization Study: part 2: Filter-based measurements of $PM_{2.5}$ and PM_{coarse} mass and composition. J. Air Waste Manage. Assoc. 55, 1527–1542.
Edgerton, E.S., Hartsell, B.E., Saylor, R.D., Jansen, J.J., Hansen, D.A., Hidy, G.M., 2006. The Southeastern Aerosol Research and Characterization Study: part 3: Continuous measurements of fine particulate matter mass and composition. J. Air Waste Manage. Assoc. 56, 1325–1341.
Edgerton, E.S., Saylor, R.D., Hartsell, B.E., Jansen, J.J., Hansen, D.A., 2007. Ammonia and ammonium measurements from the southeastern United States. Atmos. Environ. 41, 3339–3351.
Ellis, R.A., Murphy, J.G., Markovic, M.Z., VandenBoer, T.C., Makar, P.A., Brook, J., Mihele, C., 2011. The influence of gas-particle partitioning and surface-atmosphere exchange on ammonia during BAQS-Met. Atmos. Chem. Phys. 11, 133–145.
Fine, P.M., Sioutas, C., Solomon, P.A., 2008. Secondary particulate matter in the United States: Insights from the particulate matter supersites program and related studies. J. Air Waste Manage. Assoc. 58, 234–253.
Geng, G., Zhang, Q., Tong, D., Li, M., Zheng, Y., Wang, S., He, K., 2017. Chemical composition of ambient $PM_{2.5}$ over China and relationship to precursor emissions during 2005–2012. Atmos. Chem. Phys. 17, 9187–9203.
Hansen, D.A., Edgerton, E.S., Hartsell, B.E., Jansen, J.J., Kandasamy, N., Hidy, G.M., Blanchard, C.L., 2003. The Southeastern Aerosol research and characterization study: part 1–overview. J. Air Waste Manage. Assoc. 53, 1460–1471.
Hinds, W.C., 1998. Aerosol Technology: Properties, Behavior and Measurement of Airborne Particles, 2nd edition. John Wiley & Sons, New York.
Huy, D.H., Thanh, L.T., Hien, T.T., Takenaka, N., 2019. Comparative study on water-soluble inorganic ions in $PM_{2.5}$ from two distinct climate regions and air quality. J. Environ. Sci. 88, 349–360.
Khoder, M.I., 2002. Atmospheric conversion of sulfur dioxide to particulate sulfate and nitrogen dioxide to particulate nitrate and gaseous nitric acid in an urban area. Chemosphere 49, 675–684.
Li, Y., Shu, M., Ho, S.S.H., Yu, J., Yuan, Z., Liu, Z., Wang, X., Zhao, X., 2018. Effects of chemical composition of $PM_{2.5}$ on visibility in a semi-rural city of Sichuan Basin. Aerosol Air Qual. Res. 18, 957–968.
Liu, Z., Gao, W., Yu, Y., Hu, B., Xin, J., Sun, Y., Wang, L., Wang, L., Wang, G., Bi, X., Zhang, G., Xu, H., Cong, Z., He, J., Xu, J., Wang, Y., 2018. Characteristics of $PM_{2.5}$ mass concentrations and chemical species in urban and background areas of China: emerging results from CARE-China network. Atmos. Chem. Phys. 18, 8849–8871.
Ma, Y., Chen, R., Pan, G., Xu, X., Song, W., Chen, B., 2011. Fine particulate air pollution and daily mortality in Shenyang, China. Sci. Total Environ. 409, 2473–2477.
Makar, P.A., Wiebe, H.A., Staebler, R.M., Li, S.M., Anlauf, K., 1998. Measurement and modeling of particle nitrate formation. J. Geophys. Res. 103, 13095–13110.
Makar, P.A., Moran, M.D., Zheng, Q., Cousineau, S., Sassi, M., Duhamel, A., Besner, M., Davignon, D., Crevier, L.P., Bouchet, V.S., 2009. Modelling the impacts of ammonia emissions reductions on north American air quality. Atmos. Chem. Phys. Discuss. 9, 5371–5422.
McQuilling, A.M., 2016. Ammonia Emissions from Livestock in the United States: From Farm Emissions Models to a New National Inventory. Dissertation. Carnegie Mellon University.
Meng, Z., Xu, X., Lin, W., Ge, B., Xie, Y., Song, B., Jia, S., Zhang, R., Peng, W., Wang, Y., Cheng, H., Yang, W., Zhao, H., 2018. Role of ambient ammonia in particulate ammonium formation at a rural site in the North China Plain. Atmos. Chem. Phys. 18, 167–184.
Nenes, A., Pilinis, C., Pandis, S.N., 1998. ISORROPIA: a new thermodynamic equilibrium model for multiphase multicomponent inorganic aerosols. Aquat. Geochem. 4, 123–152.
Olszyna, K.J., Bairai, S.T., Tanner, R.L., 2005. Effect of ambient NH_3 levels on $PM_{2.5}$ compositions in the Great Smoky Mountains National Park. Atmos. Environ. 39, 4593–4606.
Pan, Y., Tian, S., Liu, D., Fang, Y., Zhu, X., Zhang, Q., Zheng, B., Michalski, G., Wang, Y., 2016. Fossil fuel combustion-related emissions dominate atmospheric ammonia sources during severe haze episodes: evidence from ^{15}N-stable isotope in size-resolved aerosol ammonium. Environ. Sci. Technol. 50, 8049–8056.
Pathak, R.K., Wu, W.S., Wang, T., 2009. Summertime $PM_{2.5}$ ionic species in four major cities of China: nitrate formation in an ammonia-deficient atmosphere. Atmos. Chem. Phys. 9, 1711–1722.
Perrone, M.R., Vecchi, R., Romano, S., Becagli, S., Traversi, R., Paladini, F., 2019. Weekly cycle assessment of PM mass concentrations and sources and impacts on temperature and wind speed in Southern Italy. Atmos. Res. 218, 129–144.
Phillips, S.B., Arya, S.P., Aneja, V.P., 2004. Ammonia flux and dry deposition velocity from near-surface concentration gradient measurements over a grass surface in North Carolina. Atmos. Environ. 38, 3469–3480.
Pope III, C., Ezzati, M., Dockery, D.W., 2009. Fine-particulate air pollution and life expectancy in the United States. New Engl. J. Med. 360, 376–386.
Poulain, L., Spindler, G., Birmili, W., Plass-Dulmer, C., Wiedensohler, A., Herrmann, H., 2011. Seasonal and diurnal variations of particulate nitrate and organic matter at the IfT research station Melpitz. Atmos. Chem. Phys. 11, 12579–12599.
Pui, D.Y.H., Chen, S., Zuo, Z., 2014. $PM_{2.5}$ in China: Measurements, sources, visibility and health effects, and mitigation. Particuology 13, 1–26.
Rattray, G., Sievering, H., 2001. Dry deposition of ammonia, nitric acid, ammonium, and nitrate to alpine tundra at Niwot Ridge, Colorado. Atmos. Environ. 35, 1105–1109.
Reche, C., Viana, M., Karanasiou, A., Cusack, M., Alastuey, A., Artiñano, B., Revuelta, M.A., López-Mahía, P., Blanco-Heras, G., Rodríguez, S., Campa, A.M.S., Fernández-Camacho, R., González-Castanedo, Y., Mantilla, E., Tang, Y.S., Querol, X., 2015. Urban NH_3 levels and sources in six major Spanish cities. Chemosphere 119, 769–777.
Saylor, R.D., Edgerton, E.S., Hartsell, B.E., Baumann, K., Hansen, D.A., 2010. Continuous gaseous and total ammonia measurements from the southeastern aerosol research and characterization (SEARCH) study. Atmos. Environ. 44, 4994–5004.
Saylor, R.D., Myles, L., Sibble, D., Caldwell, J., Xing, X., 2015. Recent trends in gas-phase ammonia and $PM_{2.5}$ ammonium in the Southeast United States. J. Air Waste Manage. Assoc. 65, 347–357.
Seinfeld, J.H., Pandis, S.N., 2006. Atmospheric Chemistry and Physics: From Air Pollution to Climate Change. John Wiley & Sons, New York.
Sharma, M., Kishore, S., Tripathi, S.N., Behera, S.N., 2007. Role of atmospheric ammonia in the formation of inorganic secondary particulate matter: a study at Kanpur, India. J. Atmos. Chem. 58, 1–17.
Snider, G., Weagle, C.L., Murdymootoo, K.K., Ring, A., Ritchie, Y., Stone, E., Martin, R.V., 2016. Variation in global chemical composition of $PM_{2.5}$: emerging results from SPARTAN. Atmos. Chem. Phys. 16, 9629–9653.
Song, S., Gao, M., Xu, W., Shao, J., Shi, G., Wang, S., Wang, Y., Sun, Y., McElroy, M.B., 2018. Fine-particle pH for Beijing winter haze as inferred from different thermodynamic equilibrium models. Atmos. Chem. Phys. 18, 7423–7438.
Squizzato, S., Masiol, M., Brunelli, A., Pistollato, S., Tarabotti, E., Rampazzo, G., Pavoni, B., 2013. Factors determining the formation of secondary inorganic aerosol: a case study in the Po Valley (Italy). Atmos. Chem. Phys. 13, 1927–1939.
Stokstad, E., 2014. Ammonia pollution from farming may exact hefty health costs. Sci. 343, 238.
Sutton, M.A., Asman, W.A.H., Schjorring, J.K., 1994. Dry deposition of reduced nitrogen. Tellus. 46, 255–273.
Tian, M., Wang, H., Chen, Y., Yang, F., Zhang, X., Zou, Q., Zhang, R., Ma, Y., He, K., 2016. Characteristics of aerosol pollution during heavy haze events in Suzhou, China. Atmos. Chem. Phys. 16, 7357–7371.
USEPA, 2000. Guidance for Data Quality Assessment. Available at. https://www.epa.gov/sites/production/files/2015-06/documents/g9-final.pdf.
USEPA, 2004. Estimating Ammonia Emissions from Anthropogenic Nonagricultural Sources-Draft Final Report. Available at. https://www.epa.gov/sites/production/files/2015-08/documents/eiip_areasourcesnh3.pdf.
USEPA, 2011. National Emission Inventory (NEI). Available at. https://www.epa.gov/air-emissions-inventories/2011-national-emissions-inventory-nei-data.
USEPA, 2019. $PM_{2.5}$ Precursor Demonstration Guidance. Available at. https://www.epa.gov/sites/production/files/2019-05/documents/transmittal_memo_and_pm25_precursor_demo_guidance_5_30_19.pdf.
USEPA, 2020. Particulate Matter Basics. Available at. https://www.epa.gov/pm-pollution/particulate-matter-pm-basics.
USGS, 2016. Global Change Monitoring Portal. Available at. https://my.usgs.gov/gcmp/program/show/943855.
Walker, J.T., Whitall, D.R., Robarge, W., Paerl, H.W., 2004. Ambient ammonia and ammonium aerosol across a region of variable ammonia emission density. Atmos. Environ. 38, 1235–1246.
Walker, J.T., Beachley, G., Amos, H.M., Baron, J.S., Bash, J., Baumgardner, R., Bell, M.D., Benedict, K.B., et al., 2019. Toward the improvement of total nitrogen deposition budgets in the United States. Sci. Total Environ. 691, 1328–1352.
Wang, Y., Zhuang, G., Sun, Y., An, Z., 2006. The variation of characteristics and formation mechanisms of aerosols in dust, haze, and clear days in Beijing. Atmos. Environ. 40, 6579–6591.
Wang-Li, L., 2015. Insights to the formation of secondary inorgarnic $PM_{2.5}$: current knowledge and future needs. Int. J. Agric. & Biol. Eng. 8, 1–13.
Whaley, C.H., Makar, P.A., Shephard, M.W., Zhang, L., Zhang, J., Zheng, Q., Akingunola, A., Wentworth, G.R., Murphy, J.G., Kharol, S.K., Cady-Pereira, K.E., 2018. Contributions of natural and anthropogenic sources to ambient ammonia in the Athabasca Oil Sands and North-Western Canada. Atmos. Chem. Phys. 18, 2011–2034.
Xing, J., Pleim, J., Mathur, R., Pouliot, G., Hogrefe, C., Gan, C.M., Wei, C., 2013. Historical gaseous and primary aerosol emissions in the United States from 1990 to 2010. Atmos. Chem. Phys. 13, 7531–7549.
Xu, W., Wu, Q., Liu, X., Tang, A., Dore, A.J., Heal, M.R., 2016. Characteristics of ammonia, acid gases, and $PM_{2.5}$ for three typical land-use types in the North China Plain. Environ. Sci. Pollut. Res. 23, 1158–1172.
Zhang, Y., Wu, S.-Y., Krishnan, S., Wang, K., Queen, A., Aneja, V.P., Arya, S.P., 2008. Modeling agricultural air quality: current status, major challenges and outlook. Atmos. Environ. 42, 3218–3237.
Zhang, Q., Quan, J., Tie, X., Li, X., Liu, Q., Gao, Y., Zhao, D., 2015. Effects of meteorology and secondary particle formation on visibility during heavy haze events in Beijing, China. Sci. Total Environ. 502, 578–584.